Constraints on cosmological models and reconstructing the acceleration history of the Universe with gamma-ray burst distance indicators

Nan Liang[1]
Department of Astronomy, Beijing Normal University, Beijing 100875, China

Puxun Wu[†]
Department of Physics and Institute of Physics, Hunan Normal University, Changsha, Hunan 410081, China

Shuang Nan Zhang[‡]
Key Laboratory of Particle Astrophysics, Institute of High Energy Physics, Chinese Academy of Sciences, Beijing 100049, China and Physics Department, University of Alabama in Huntsville, Huntsville, Alabama 35899, USA

(Received 10 December 2009; published 15 April 2010)

Gamma-ray bursts (GRBs) have been regarded as standard candles at very high redshift for cosmology research. We have proposed a new method to calibrate GRB distance indicators with Type Ia supernova (SNe Ia) data in a completely cosmology-independent way to avoid the circularity problem that had limited the direct use of GRBs to probe cosmology [N. Liang, W. K. Xiao, Y. Liu, and S. N. Zhang, Astrophys. J. **685**, 354 (2008).]. In this paper, a simple method is provided to combine GRB data into the joint observational data analysis to constrain cosmological models; in this method those SNe Ia data points used for calibrating the GRB data are not used to avoid any correlation between them. We find that the ΛCDM model is consistent with the joint data in the 1-σ confidence region, using the GRB data at high redshift calibrated with the interpolating method, the Constitution set of SNe Ia, the cosmic microwave background radiation from Wilkinson Microwave Anisotropy Probe five year observation, the baryonic acoustic oscillation from the spectroscopic Sloan Digital Sky Survey Data Release 7 galaxy sample, the x-ray baryon mass fraction in clusters of galaxies, and the observational Hubble parameter versus redshift data. Comparing to the joint constraints with GRBs and without GRBs, we find that the contribution of GRBs to the joint cosmological constraints is a slight shift in the confidence regions of cosmological parameters to better enclose the ΛCDM model. Finally, we reconstruct the acceleration history of the Universe up to $z > 6$ with the distance moduli of SNe Ia and GRBs and find some features that deviate from the ΛCDM model and seem to favor oscillatory cosmology models; however, further investigations are needed to better understand the situation.

DOI: 10.1103/PhysRevD.81.083518 PACS numbers: 98.80.Es, 98.80.−k, 98.80.Jk

I. INTRODUCTION

Gamma-ray bursts (GRBs) are the most intense explosions observed so far and likely to occur in high redshift range. Recently, GRB 090423 has been observed at a very high redshift, $z > 8$ [1]. The early universe can be explored by using GRBs at the high redshift, which is hardly achievable by Type Ia supernova (SNe Ia). In recent years, several GRB luminosity relations between measurable properties of the prompt gamma-ray emission with the luminosity or energy have been proposed as distance indicators, many of which are the two-dimensional (2D) luminosity relations, such as the isotropic energy ($E_{\rm iso}$)—peak spectral energy ($E_{\rm peak}$) relation (i.e., the so-called Amati relation) [2], the luminosity (L)—spectral lag ($\tau_{\rm lag}$) relation [3], the L—variability (V) relation [4], the L-$E_{\rm peak}$ relation [5], the L—minimum rise time ($\tau_{\rm RT}$) relation [6], and the collimation-corrected energy (E_γ)-$E_{\rm peak}$ relation (i.e., the so-called Ghirlanda relation) with small scattering [7]. In order to reduce the large scattering in some of these 2D relations, several 3D luminosity relations are also presented [8–10]. Liang and Zhang first proposed the relation among $E_{\rm iso}$, $E_{\rm peak}$, and t_b (i.e., the so-called Liang-Zhang relation) [8], where t_b is the break time of the optical afterglow light curves; and Firmani *et al.* found the relation among L, $E_{\rm peak}$, and $T_{0.45}$ (i.e., the so-called Firmani relation) [9], where $T_{0.45}$ is the "high-signal" time scale of the prompt emission. Both of the 3D luminosity relations above could reduce the scattering in the luminosity or energy *versus* the $E_{\rm peak}$ relation. More recently, Yu *et al.* find that, for the 3D luminosity relations between the luminosity and an energy scale $E_{\rm peak}$ and a time scale ($\tau_{\rm lag}$ or $\tau_{\rm RT}$), the intrinsic scattering is considerably smaller than that of those corresponding 2D luminosity relations [10]. Other GRB luminosity relations have been proposed in many works [11–13]. For reviews of GRB luminosity relations, see e.g. [14–17].

However, all the luminosity relations of GRBs presented above are always empirical, but still without solid physical interpretations [16]. Moreover, the luminosity relations

*liangn@bnu.edu.cn
†wpx0227@gmail.com
‡zhangsn@ihep.ac.cn

cannot be calibrated with a sufficiently large low-redshift GRB sample. Therefore previous calibrations have been usually obtained by assuming a particular cosmological model. Once these GRB luminosity relations are calibrated, GRB data could be considered as standard candles at very high redshift for cosmology research [8,9,16–34] (see e.g. [16,17] for reviews). In 2003, Schaefer derived the luminosity distances of nine GRBs with known redshifts by using two GRB luminosity relations (L-$\tau_{\rm lag}$, L-V) to construct the first GRB Hubble diagram [18]. For 16 GRBs with redshift measurements, Bloom *et al.* found a narrow clustering of geometrically corrected gamma-ray energies within the framework of the uniform conical jet model [19]. Dai *et al.* proposed an approach to consider the Ghirlanda relation to constrain cosmological parameters and dark energy [20]. Because of the small scatter, the 3D luminosity relations have been used for cosmological constraint, including the Liang-Zhang relation [8], and the Firmani relation [24,35]. In 2007, Schaefer used five 2D relations (L-$\tau_{\rm lag}$, L-V, L-$E_{\rm peak}$, L-$\tau_{\rm RT}$, and E_γ-$E_{\rm peak}$) to construct the Hubble diagram of 69 GRBs [17]. These GRB data have been widely used to constrain cosmology and dark energy models in many recent works [27,28], and joint constraints by combining these GRB data with SNe Ia and the other cosmological probes have been derived in [29–32]. Instead of a hybrid sample over the whole redshift range of GRBs, Takahashi *et al.* [33] first calibrated GRB relations (L-$\tau_{\rm lag}$, L-V) at low redshift where distance-redshift relations have been already determined from SNe Ia. This method was adopted by Bertolami and Silva for considering the use of GRBs at $1.5 < z < 5$ calibrated with the bursts at $z \leq 1.5$ as distance markers to study the generalized Chaplygin gas model [34]. All the calibration methods above carried out have been derived usually from the ΛCDM model with particular model parameters according to the concordance cosmology.

An important point related to the use of GRBs for cosmology is the dependence on the cosmological model in the calibration of GRB relations, which had limited the direct use of GRBs for cosmology research. In order to investigate cosmology, the relations of standard candles should be calibrated in a cosmology-independent way; otherwise, the circularity problem cannot be avoided easily [16]. Recently, the possibility of calibrating GRBs in a low dispersion in redshift near a fiducial redshift has been proposed [36,37], which has been developed further based on Bayesian theory [38]. However, the GRB sample available now is far from what is needed to calibrate the relations in this way [16,38]. Many of the works treat the circularity problem with statistical approaches [18,23,39–41]. A simultaneous fit of the parameters in the calibration curves and the cosmology is carried out to find the optimal GRB relation and the optimal cosmological model in the sense of a minimum scattering in both the luminosity relations and the Hubble diagram [18]. Firmani *et al.* proposed a Bayesian method to get around the circularity problem [23]. Li *et al.* presented a global fitting analysis for the Ghirlanda relation to deal with the problem [39]. Amati *et al.* used the $E_{\rm iso}$-$E_{\rm peak}$ relation to measure the cosmological parameter by adopting a maximum likelihood approach [40]. More recently, Wang has shown that the current GRB data can be summarized by a set of model independent distance measurements, with negligible loss of information [41], which is followed by [42–44]. However, an input cosmological model is still required in doing the joint fitting, the circularity problem cannot be circumvented completely by means of these statistical approaches.

In our previous paper [45], we presented a new method to calibrate several GRB luminosity relations in a completely cosmology-independent manner. Our method avoids the circularity problem more clearly than previous cosmology-dependent calibration methods. It is obvious that objects at the same redshift should have the same luminosity distance in any cosmology. Therefore, the luminosity distance at any redshift in the redshift range of SNe Ia can be obtained by interpolating (or by other mathematical approach) directly from the SNe Ia Hubble diagram. Using the interpolation method, we calibrated seven GRB luminosity relations (L-$\tau_{\rm lag}$, L-V, L-$E_{\rm peak}$, L-$\tau_{\rm RT}$, E_γ-$E_{\rm peak}$, $E_{\rm iso}$-$E_{\rm peak}$, and $E_{\rm iso}$-$E_{\rm peak}$-t_b) with the data compiled by Schaefer [17]. Then if further assuming these calibrated GRB relations valid for all long GRB data, we can use the standard Hubble diagram method to constrain the cosmological parameters from the GRB data at high redshift obtained by utilizing the relations [45]. These distance data of GRBs are so far the most cosmology-independent GRB distance indicators. Following this cosmology-independent GRB calibration method from SN Ia [45], the derived GRB data at high redshift range can be used to constrain cosmological models without circularity problem [45–50]. Capozziello and Izzo first used the $E_{\rm iso}$-$E_{\rm peak}$-t_b relation and the E_γ-$E_{\rm peak}$ relation calibrated with the so-called Liang method to derive the related cosmography parameters [deceleration parameters (q), jerk parameters (j), and snap parameters (s) [51]], which are only related to the derivatives of the scale factor without any *a priori* assumption [46]. Wei and Zhang used the Amati relation calibrated with the interpolation method to reconstruct the acceleration history of the Universe and constrain cosmological models [48,49].

Furthermore, we proposed another approach to calibrate GRB relations by using an iterative procedure [52], which is a nonparametric method in a model independent manner to reconstruct the luminosity distance at any redshift in the redshift range of SNe Ia [53–55]. Similar to the interpolation method, Cardone *et al.* constructed an updated GRBs Hubble diagram on six 2D relations calibrated by local regression from SNe Ia [56]. This method and GRB data have been used to cosmological constraints with SNe Ia in

some following works [42,57]. Kodama *et al.* presented that the L-$E_{\rm peak}$ relation can be calibrated with the empirical formula fitted from the luminosity distance of SNe Ia [58]. This method has been used to constrain cosmological parameters by combining these GRB data with SNe Ia in a following work [59]. However, it is noted that this calibration procedure depends seriously on the choice of the formula and various possible formulas can be fitted from the SNe Ia data that could give different calibration results of GRBs. As the cosmological constraints from GRBs are sensitive to GRBs calibration results [41], the reliability of this method should be tested carefully. Moreover, as pointed out in [41], the GRB luminosity relations that are calibrated by this way are no longer completely independent of all the SNe Ia data points; therefore these GRB data cannot be used to directly combine with the whole SNe Ia data set to constrain cosmological parameters and dark energy.

It is easy to find that the number of SNe Ia data points that have been used in the linear interpolating procedure to obtain the GRB data is relatively small compared to the whole SNe Ia sample. In order to combine GRB data obtained by our interpolation method into the joint observational data analysis to constrain cosmological models, we can exclude the SNe points that have been used in the interpolating procedure from the SNe Ia sample used to the joint constraints. In this work, with the updated distance moduli of the 42 GRBs at $z > 1.4$ obtained by the interpolating method [45] from the Union set of 307 SNe Ia [60], we provide a simple method to ensure that the calibrated GRB data are independent of the SNe Ia data used in the joint data fitting to constrain cosmological models, by using the Constitution set of 397 SNe Ia [61], along with the cosmic microwave background radiation (CMB) observation from the five-year Wilkinson Microwave Anisotropy Probe (WMAP5) result [62], (R, l_a, $\Omega_b h^2$); the baryonic acoustic oscillation (BAO) [63] observation from the spectroscopic Sloan Digital Sky Survey (SDSS) Data Release 7 (DR7) galaxy sample [64] ($d_{0.2}$, $d_{0.35}$); the 26 baryon mass fraction in clusters of galaxies (CBF) from the x-ray gas observation ($f_{\rm gas}$) [65]; and the 11 Hubble parameter versus redshift data, $H(z)$ [66,67]. Our goal is to determine the contribution of GRBs to the joint cosmological constraints in the confidence regions of cosmological parameters by comparing to the joint constraints with GRBs and without GRBs. Finally we also reconstruct the acceleration history of the Universe up to $z > 6$ with the distance moduli of SNe Ia and GRBs.

II. OBSERVATIONAL DATA ANALYSIS

The updated distance moduli of the 42 GRBs at $z > 1.4$ are obtained by the five GRB luminosity relations that are calibrated from the 27 GRBs at $z < 1.4$ with the interpolating method [45] using the Union set of 307 SNe Ia [60]. The Union set includes the Supernova Legacy Survey [68] and the ESSENCE Survey [69], the extended data set of distant SNe Ia observed with the Hubble Space Telescope [70], and the formerly observed SNe Ia data. For the SNe data in joint analysis, we use the new Constitution set of 397 SNe Ia [61], which combine 90 CfA3 SNe Ia samples with the Union set [60]. We also consider the shift parameters set (R, l_a, $\Omega_b h^2$) [62], the BAO [63] parameters set ($d_{0.2}$, $d_{0.35}$) from SDSS DR7 [64], the 26 $f_{\rm gas}$ data from the x-ray gas observation in clusters of galaxies [65], and the 11 $H(z)$ data from the differential ages of passively evolving galaxies [66] and from the BAO peak position [67].

In our previous paper [45], we used the data for 69 GRBs compiled by Schaefer [17] and adopted the data for 192 SNe Ia compiled by Davis *et al.* [71] to calibrate seven GRB luminosity relations (L-$\tau_{\rm lag}$, L-V, L-$E_{\rm peak}$, L-$\tau_{\rm RT}$, E_γ-$E_{\rm peak}$, $E_{\rm iso}$-$E_{\rm peak}$, and $E_{\rm iso}$-$E_{\rm peak}$-t_b) at $z \leq 1.4$ by using the interpolation method. In this work, we use the Union set of 307 SNe Ia [60] to determine the values of the intercepts and the slopes of GRBs luminosity relations calibrated with the GRB sample at $z \leq 1.4$ by using the linear interpolation method. We do not include the 90 SNe Ia data from CfA3 [61] due to their extremely low redshift ($z < 0.1$), which would not affect the calibrated results for GRB luminosity relations at $0.17 \leq z \leq 1.4$. The 2D luminosity relation of GRBs can be generally written in the form

$$\log y = a + b \log x, \tag{1}$$

where y is the luminosity (L/erg s^{-1}) or energy (E_γ/erg); x is the GRB parameters measured in the rest frame, e.g., $\tau_{\rm lag}(1+z)^{-1}/(0.1{\rm s})$, $V(1+z)/0.02$, $E_{\rm peak}(1+z)/(300\ {\rm keV})$, $\tau_{\rm RT}(1+z)^{-1}/(0.1{\rm s})$, for the corresponding 2D relations. We adopt the data for these quantities from Ref. [17] including five 2D GRB luminosity relations (L-$\tau_{\rm lag}$, L-V, L-$E_{\rm peak}$, L-$\tau_{\rm RT}$, and E_γ-$E_{\rm peak}$). For the E_γ-$E_{\rm peak}$ relation, in order to calculate the total collimation-corrected energy E_γ, one needs to know the beaming factor, $F_{\rm beam} = (1 - \cos\theta_{\rm jet})$, where the value of the jet opening angle $\theta_{\rm jet}$ is related to the jet break time (t_b) and the isotropic energy for an Earth-facing jet, $E_{\gamma,{\rm iso},52} = E_{\gamma,{\rm iso}}/10^{52}$ erg [72]. When calculating $E_{\gamma,{\rm iso}}$, we also use the interpolation method from SNe Ia to avoid the circularity problem. We determine the values of the intercept (a) and the slope (b) with their 1-σ uncertainties calibrated with the GRB sample at $z \leq 1.4$ by using the linear interpolation methods from the Union set of 307 SNe Ia.

Further assuming that these GRB luminosity relations do not evolve with redshift, we are able to obtain the luminosity (L) or energy (E_γ) of each burst at high redshift ($z > 1.4$). Therefore, the luminosity distance (d_L) can be derived. A distance modulus can be calculated as $\mu = 5\log(d_L/{\rm Mpc}) + 25$. The weighted average distance modulus from the five relations for each GRB is $\mu = (\sum_i \mu_i/\sigma_{\mu_i}^2)/(\sum_i \sigma_{\mu_i}^{-2})$, with its uncertainty $\sigma_\mu = (\sum_i \sigma_{\mu_i}^{-2})^{-1/2}$, where the summations run from 1 to 5 over

the five relations with available data. For more details of the calculation, see [17,45]. We have plotted the Hubble diagram of 397 SNe Ia [61] which combine 90 CfA3 SNe Ia samples with the Union set [60] and the 69 GRBs obtained using the interpolation methods in Fig. 1. The distance moduli of the 27 GRBs at $z \leq 1.4$ are obtained by using the linear interpolation method directly from the Union SNe data. The 42 GRB data at $z > 1.4$ are obtained by utilizing the five relations calibrated with the sample at $z \leq 1.4$ using the interpolation method.

Constraints from the SNe Ia data and the GRB data can be obtained by fitting the distance moduli $\mu(z)$. A distance modulus can be calculated as

$$\mu = 5\log\frac{d_L}{\mathrm{Mpc}} + 25 = 5\log_{10}D_L - \mu_0, \tag{2}$$

where $\mu_0 = 5\log_{10}h + 42.38$, $h = H_0/(100\ \mathrm{km/s/Mpc})$, H_0 is the Hubble constant, and the luminosity distance D_L can be calculated by

$$D_L \equiv H_0 d_L = (1+z)\Omega_k^{-1/2}\mathrm{sinn}\left[\Omega_k^{1/2}\int_0^z \frac{dz'}{E(z')}\right], \tag{3}$$

where $\Omega_k = 1 - \Omega_{\mathrm{M0}} - \Omega_{\mathrm{DE}}$, sinn$(x)$ is sinh for $\Omega_k > 0$, sin for $\Omega_k < 0$, and x for $\Omega_k = 0$; and $E(z)$ can be given by

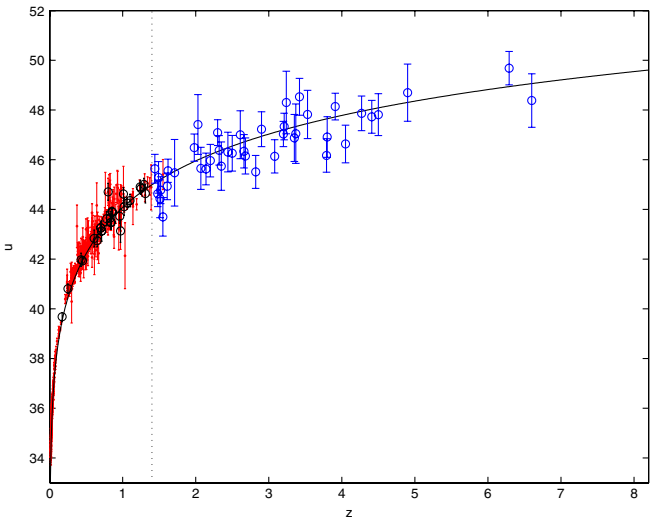

FIG. 1 (color online). Hubble Diagram of 397 SNe Ia (red dots) and the 69 GRBs (circles) obtained using the interpolation methods. The 27 GRBs at $z \leq 1.4$ are obtained by linear interpolating from SNe Ia data (black circles), and the 42 GRBs at $z > 1.4$ (blue circles) are obtained with the five relations calibrated with the sample at $z \leq 1.4$ using the interpolation method. The curve is the theoretical distance modulus in the concordance model ($w = -1$, $\Omega_{\mathrm{M0}} = 0.27$, $\Omega_\Lambda = 0.73$), and the vertical dotted line represents $z = 1.4$.

$$E(z) \equiv \frac{H}{H_0} = \left[\Omega_{\mathrm{M0}}(1+z)^3 + \Omega_{\mathrm{DE}}\exp\left[3\int_0^z \frac{1+w(z')}{1+z'}dz'\right] + \Omega_k(1+z)^2\right]^{1/2}, \tag{4}$$

where the equation of state (*EoS*) of dark energy $w(z)$ is determined by the choice of the specific dark energy model. The χ^2 value of the observed distance moduli can be calculated by

$$\chi^2_\mu = \sum_{i=1}^{N}\frac{[\mu_{\mathrm{obs}}(z_i) - \mu(z_i)]^2}{\sigma^2_{\mu,i}}, \tag{5}$$

where $\mu_{\mathrm{obs}}(z_i)$ is the observed distance modulus for the SNe Ia and/or GRBs at redshift z_i with its error σ_{μ_i}; $\mu(z_i)$ is the theoretical value of distance modulus from a dark energy model, which can be calculated from Eqs. (2)–(4). The nuisance parameter μ_0 (or h) can be obtained by marginalizing the likelihood functions of over μ_0 (or h) for all values [20] or treated by following an effective approach [73] to expand the χ^2_μ to $\chi^2_\mu(\mu_0) = A\mu_0^2 - 2B\mu_0 + C$, with $A = \sum 1/\sigma^2_{\mu_i}$, $B = \sum[\mu_{\mathrm{obs}}(z_i) - 5\log_{10}D_L]/\sigma^2_{\mu_i}$, and $C = \sum[\mu_{\mathrm{obs}}(z_i) - 5\log_{10}D_L]^2/\sigma^2_{\mu_i}$. Thus the χ^2_μ has a minimum value for $\mu_0 = B/A$ at $\hat{\chi}^2_\mu$, which is given by

$$\hat{\chi}^2_\mu = C - \frac{B^2}{A}. \tag{6}$$

Therefore we can minimize $\hat{\chi}^2_\mu$ instead of minimizing χ^2_μ.

For the CMB observation from the WMAP5 results [62], the two shift parameters R and l_a, together with the baryon density fraction of the Universe ($\omega_b = \Omega_b h^2$) can provide an efficient summary of CMB data to constrain cosmological models. The shift parameter R can be expressed as

$$R = \Omega_{\mathrm{M0}}^{1/2}\Omega_k^{-1/2}\mathrm{sinn}\left[\Omega_k^{1/2}\int_0^{z_{\mathrm{rec}}}\frac{dz}{E(z)}\right], \tag{7}$$

where z_{rec} is the redshift of recombination, which is given by [74] $z_{\mathrm{rec}} = 1048[1 + 0.00124\omega_b^{-0.738}(1 + g_1(\Omega_{\mathrm{M0}}h^2)^{g_2})]$, $g_1 = 0.0783\omega_b^{-0.238}(1 + 39.5\omega_b^{-0.763})^{-1}$, and $g_2 = 0.560(1 + 21.1\omega_b^{1.81})^{-1}$. The shift parameter l_a can be expressed as

$$l_a = \pi\frac{\Omega_k^{-1/2}\mathrm{sinn}[\Omega_k^{1/2}\int_0^{z_{\mathrm{rec}}}\frac{dz}{E(z)}]/H_0}{r_s(z_{\mathrm{rec}})}, \tag{8}$$

where $r_s(z_{\mathrm{rec}})$ is the comoving sound horizon at photo-decoupling epoch,

$$r_s(z_{\rm rec}) = \frac{1}{H_0}\int_{z_{\rm rec}}^{\infty}\frac{c_s(z)}{E(z)}dz = a_{\rm rec}\int_0^{a_{\rm rec}}\frac{c_s}{\Omega_{\rm M0}^{1/2}}\left[\frac{\Omega_r h^2}{\Omega_{\rm M0}h^2}+a\right]^{-1/2}da, \quad (9)$$

with the sound speed $c_s = (1/\sqrt{3})[1 + a(31\,500\omega_b(T_{\rm CMB}/2.7\ k)^{-4})]^{-1/2}$ [44], and $T_{\rm CMB} = 2.725\ k$ [62]. From the WMAP5 measurement, the best-fit values of $(R, l_a, 100\omega_b)$ for a flat prior are [62]

$$\bar{\mathbf{P}}_{\rm CMB} = \begin{pmatrix}\bar{R}\\ \bar{l}_a\\ 100\omega_b\end{pmatrix} = \begin{pmatrix}1.710 \pm 0.019\\ 302.10 \pm 0.86\\ 2.2765 \pm 0.0596\end{pmatrix}. \quad (10)$$

The χ^2 value of the CMB observation from WMAP5 can be expressed as

$$\chi^2_{\rm CMB} = \Delta\mathbf{P}^T_{\rm CMB}\mathbf{C}_{\rm CMB}{}^{-1}\Delta\mathbf{P}_{\rm CMB}, \quad (11)$$

where

$$\Delta\mathbf{P}_{\rm CMB} = \begin{pmatrix}R - 1.710\\ l_a - 302.10\\ 100\omega_b - 2.2765\end{pmatrix}, \quad (12)$$

and the corresponding inverse covariance matrix is [62]

$$\mathbf{C}_{\rm CMB}{}^{-1} = \begin{pmatrix}2809.73 & -0.133\,381 & 158.356\\ -0.133\,381 & 2.219\,08 & 19.7195\\ 158.356 & 19.7195 & 465.728\end{pmatrix}. \quad (13)$$

It is noted that we use the priors following [75], $\Omega_b = 0.022765/h^2$ and $h = 0.705$ [62], when calculating the value of $\chi^2_{\rm CMB}$.

For the BAO observation [63], from the SDSS DR7 galaxy sample [64], we use the measurement of d_z at $z = 0.2$ and $z = 0.35$, where d_z can be expressed as [64]

$$d_z = \frac{r_s(z_d)}{D_V(z_{\rm BAO})}, \quad (14)$$

where z_d is the drag epoch at which baryons were released from photons, which is given by [76] $z_d = 1291(\Omega_{\rm M0}h^2)^{0.251}[(1 + b_1\omega_b^{b_2})]/[1 + 0.659(\Omega_{\rm M0}h^2)^{0.828}]$, $b_1 = 0.313(\Omega_{\rm M0}h^2)^{-0.419}[1 + 0.607(\Omega_{\rm M0}h^2)^{0.674}]^{-1}$, and $b_2 = 0.238(\Omega_{\rm M0}h^2)^{0.223}$, and D_V can be given by [63]

$$D_V(z_{\rm BAO}) = \frac{1}{H_0}\left[\frac{z_{\rm BAO}}{E(z_{\rm BAO})}\left(\int_0^{z_{\rm BAO}}\frac{dz}{E(z)}\right)^2\right]^{1/3}. \quad (15)$$

From the SDSS DR7 measurement, the best-fit values are [64]

$$\bar{\mathbf{P}}_{\rm BAO} = \begin{pmatrix}\bar{d}_{0.2}\\ \bar{d}_{0.35}\end{pmatrix} = \begin{pmatrix}0.1905 \pm 0.0061\\ 0.1097 \pm 0.0036\end{pmatrix}. \quad (16)$$

The χ^2 value of the BAO observation from SDSS DR7 can be expressed as [64]

$$\chi^2_{\rm BAO} = \Delta\mathbf{P}^T_{\rm BAO}\mathbf{C}_{\rm BAO}{}^{-1}\Delta\mathbf{P}_{\rm BAO}, \quad (17)$$

where

$$\Delta\mathbf{P}_{\rm BAO} = \begin{pmatrix}d_{0.2} - 0.1905\\ d_{0.35} - 0.1097\end{pmatrix}, \quad (18)$$

and the corresponding inverse covariance matrix is [64]

$$\mathbf{C}_{\rm BAO}{}^{-1} = \begin{pmatrix}30\,124 & -17\,227\\ -17\,227 & 86\,977\end{pmatrix}. \quad (19)$$

The baryon mass fraction in CBF from the x-ray gas observation can be used to constrain cosmological parameters on the assumption that the gas mass fraction in clusters is a constant and thus independent of redshift. The baryon gas mass fraction $f_{\rm gas}$ can be presented as [65]

$$f_{\rm gas}(z) = \lambda\left[\frac{d_A^{\rm SCDM}(z)}{d_A(z)}\right]^{2/3}, \quad (20)$$

where $\lambda = [b\Omega_b(2h)^{3/2}]/[(1 + a)\Omega_{\rm M0}]$, $a = 0.19\sqrt{h}$, b is a bias factor motivated by gas dynamical simulations, and $d_A \equiv d_L/(1 + z)^2$ is the theoretical value of the angular diameter distance from cosmological models, $d_A^{\rm SCDM}$ is the angular diameter distance corresponding to the standard cold dark matter (SCDM) universe ($\Omega_{\rm M0} = 1$ for a flat universe). Here we adopt the usually used 26 observational $f_{\rm gas}$ data [65] to constrain cosmological models. The χ^2 value of cluster's baryon gas mass fraction is

$$\chi^2_{\rm CBF} = \sum_{i=1}^{N=26}\frac{[f_{\rm gas}^{\rm obs}(z_i) - f_{\rm gas}(z_i)]^2}{\sigma^2_{f_{{\rm gas},i}}}. \quad (21)$$

Following [77,78], we treat λ as a nuisance parameter to expand the $\chi^2_{\rm CBF}$ to $\chi^2_{\rm CBF}(\lambda) = A\lambda^2 - 2B\lambda + C$, with $A = \sum[\tilde{f}_{{\rm gas},i}/\sigma_{f_{{\rm gas},i}}]^2$, $B = \sum[\tilde{f}_{{\rm gas},i}f_{{\rm gas},i}]/\sigma^2_{f_{{\rm gas},i}}$, and $C = \sum[f_{{\rm gas},i}/\sigma_{f_{{\rm gas},i}}]^2$, where $\tilde{f}_{{\rm gas},i} = [d_A^{\rm SCDM}(z)/d_A(z)]^{2/3}$. Thus the $\chi^2_{\rm CBF}$ has a minimum value at $\hat{\chi}^2_{\rm CBF}$, which is given by

$$\hat{\chi}^2_{\rm CBF} = C - \frac{B^2}{A}. \quad (22)$$

The Hubble parameter $H(z)$ can be derived from the derivative of redshift with respect to the cosmic time,

$$H(z) = -\frac{1}{1+z}\frac{dz}{dt}. \quad (23)$$

From the Gemini Deep Deep Survey (GDDS) [79] observations of differential ages of passively evolving galaxies and other archival data [80], the $H(z)$ data at nine different redshifts ($0.09 \le z \le 1.75$) have been obtained [66]. Recently, using the BAO peak position as a standard ruler in the radial direction, $H = 83.2 \pm 2.1$ km/s/Mpc at $z = 0.24$ and $H = 90.3 \pm 2.5$ km/s/Mpc at $z = 0.43$ have been obtained [67]. To constrain cosmological models, the χ^2 value of the 11 $H(z)$ data is

$$\chi^2_H = \sum_{i=1}^{N=11} \frac{[H_{\rm obs}(z_i) - H(z_i)]^2}{\sigma^2_{H,i}}. \quad (24)$$

The nuisance parameter H_0 is also marginalized following the procedure used in calculating $\hat{\chi}^2_\mu$ and $\hat{\chi}^2_{\rm CBF}$ [73,77,78].

III. CONSTRAINTS ON COSMOLOGICAL MODELS FROM THE JOINT DATA WITH GRBS

The distance moduli of the 42 GRBs at $z > 1.4$ are obtained by the five GRB luminosity relations that are calibrated from the 27 GRBs at $z < 1.4$ with the interpolating method using directly the distance moduli of adjacent SNe Ia. In the interpolating procedure to obtain the distance moduli of the 27 GRBs at $z < 1.4$, we have used only 40 SNe Ia data points from the Union set of 307 SNe Ia. In order to combine GRB data into the joint observational data analysis to constrain the dark energy models, we exclude the 40 SNe points from the SNe Ia sample used to the joint constraints. Therefore the remaining SNe Ia data points are completely independent of the distance moduli of the 42 GRBs at $z > 1.4$. Those excluded 40 SNe are listed in the Appendix. Since the reduced 357 SNe Ia, 42 GRBs, CMB, BAO, as well as CBF and $H(z)$ are all effectively independent, we can combine the results by simply multiplying the likelihood functions. Thus the cosmological parameters can be fitted with the combined observable data by the minimum χ^2 method. The total χ^2 with the SNe + GRBs + CMB + BAO + CBF + $H(z)$ data set is

$$\chi^2 = \hat{\chi}^2_{\mu,\{\rm SN+GRB\}} + \chi^2_{\rm CMB} + \chi^2_{\rm BAO} + \hat{\chi}^2_{\rm CBF} + \hat{\chi}^2_H. \quad (25)$$

The best-fit values for these parameters can be determined by minimizing the total χ^2. For comparison, SNe + CMB + BAO + CBF + $H(z)$ without GRBs have been used to show the contribution of GRBs to the joint cosmological constraints, and we also consider the joint constraints with 397 SNe + CMB + BAO + CBF + $H(z)$. In addition, some different data sets such as SNe + GRBs + CMB + BAO, SNe + GRBs + CMB, and SNe + GRBs + BAO have also been used in the cosmological constraints.

We use the Akaike information criterion (AIC) [81] and the Bayesian information criterion (BIC, the so-called Schwarz information criterion) [82] to select the best-fit models. Liddle examined the use of information criteria in the context of cosmological observations [83]. The AIC is defined as [81] AIC $= -2\ln\mathcal{L}_{\rm max} + 2k$, where $\mathcal{L}_{\rm max}$ is the maximum likelihood and k the number of parameters of the model. Models with too few parameters give a poor fit to the data and hence have a low log-likelihood, while those with too many are penalized by the second term. The best model is the model that minimizes the AIC [83]. The BIC can be defined as [82] BIC $= -2\ln\mathcal{L}_{\rm max} + k\ln N$, where N is the number of data points used in the fit. Note that for Gaussian errors, $\chi^2_{\rm min} = -2\ln\mathcal{L}_{\rm max}$, and the difference in BIC can be simplified to BIC $= \Delta\chi^2_{\rm min} + \Delta k \ln N$. The AIC gives results similar to the BIC approach, although the AIC is not strict enough on models with extra parameters for any reasonably sized data set ($\ln N > 2$). Therefore, for comparing cosmological models from the joint data set, we only compare ΔBIC measured with respect to the best model. A difference in BIC of 2 is considered positive evidence against the model with the higher BIC, while a ΔBIC of 6 is considered strong evidence [83].

The combined data sets are used to constrain cosmological parameters and dark energy. Here we consider three cosmological models, the ΛCDM model with dark energy *EoS* $w \equiv -1$, the wCDM model with a constant *EoS*, and the Chevallier-Polarski-Linder (CPL) model in which dark energy with a parametrization *EoS* as [84]

$$w(z) = w_0 + w_a(1-a) = w_0 + w_a\frac{z}{1+z}. \quad (26)$$

For the ΛCDM model, Eq. (4) becomes

$$E(z) = [\Omega_{\rm M0}(1+z)^3 + \Omega_\Lambda - \Omega_k(1+z)^2]^{1/2}, \quad (27)$$

where $\Omega_{\rm M0} + \Omega_\Lambda + \Omega_k = 1$. For the wCDM model with a constant *EoS* for a flat universe prior,

$$E(z) = [\Omega_{\rm M0}(1+z)^3 + (1-\Omega_{\rm M0})(1+z)^{3(1+w_0)}]^{1/2}, \quad (28)$$

and considering $w(z)$ as the CPL parametrization model for a flat universe prior, Eq. (4) becomes

$$E(z) = [\Omega_{\rm M0}(1+z)^3 + (1-\Omega_{\rm M0})(1+z)^{3(1+w_0+w_a)}e^{-3w_a z/1+z}]^{1/2}. \quad (29)$$

In Fig. 2, we show the joint confidence regions in the ($\Omega_{\rm M0}$, Ω_Λ) plane for the ΛCDM model. With 357 SNe + GRBs + CMB + BAO + CBF + $H(z)$, the 1-σ confidence region for ($\Omega_{\rm M0}$, Ω_Λ) of the ΛCDM model are $(\Omega_{\rm M0}, \Omega_\Lambda) = (0.275^{+0.016}_{-0.015}, 0.723^{+0.017}_{-0.016})$, with $\chi^2_{\rm min} = 494.476$ for 438 degrees of freedom. For comparison, fitting results from the joint data without GRBs are also given in Fig. 2. With 357 SNe + CMB + BAO + CBF + $H(z)$, the best-fit values are $(\Omega_{\rm M0}, \Omega_\Lambda) = (0.270^{+0.016}_{-0.015}, 0.730^{+0.017}_{-0.017})$ with $\chi^2_{\rm min} = 449.001$ for 396 degrees of freedom. We present the best-fit value of $\Omega_{\rm M0}$, Ω_Λ with 1σ uncertainties, and $\chi^2_{\rm min}$, $\chi^2_{\rm min}$/dof, as well as AIC, BIC for the ΛCDM model in Table I.

From comparing to the joint constraints with GRBs and without GRBs, we can see that the contribution of GRBs to the joint cosmological constraints is a slight shift between the best-fit values near the line that represents a flat universe, toward a higher matter density Universe by $\Delta\Omega_{\rm M0} = 0.005$, compared to the joint constraints without GRBs. It is noted that the obtained errors for these parameters with and without GRBs are essentially unchanged, because the number of SNe Ia data points dropped is

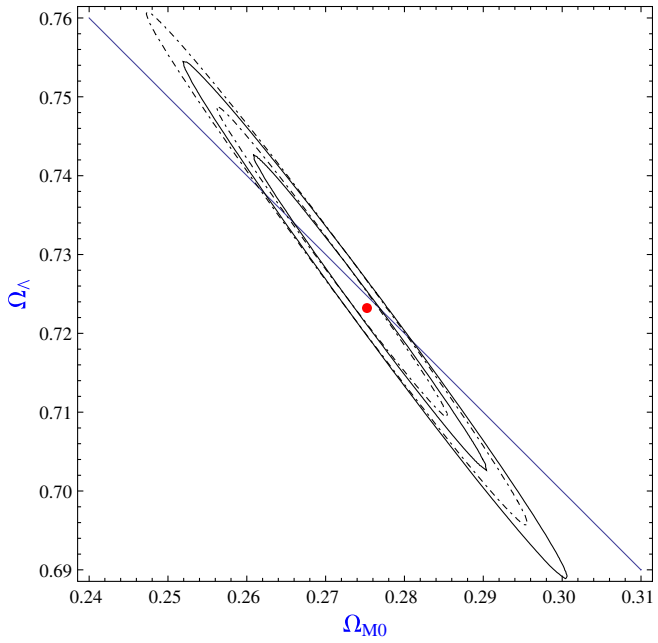

FIG. 2 (color online). The joint confidence regions in the (Ω_{M0}, Ω_Λ) plane for the ΛCDM model with SNe + GRBs + CMB + BAO + CBF + $H(z)$. The contours correspond to 1-σ and 2-σ confidence regions, and the red point is the best-fit value [SNe + GRBs + CMB + BAO + CBF + $H(z)$]. The results for the cases with and without GRBs are indicated by the solid lines and the dot-dashed lines, respectively. The blue line represents a flat universe ($\Omega_{M0} + \Omega_\Lambda = 1$).

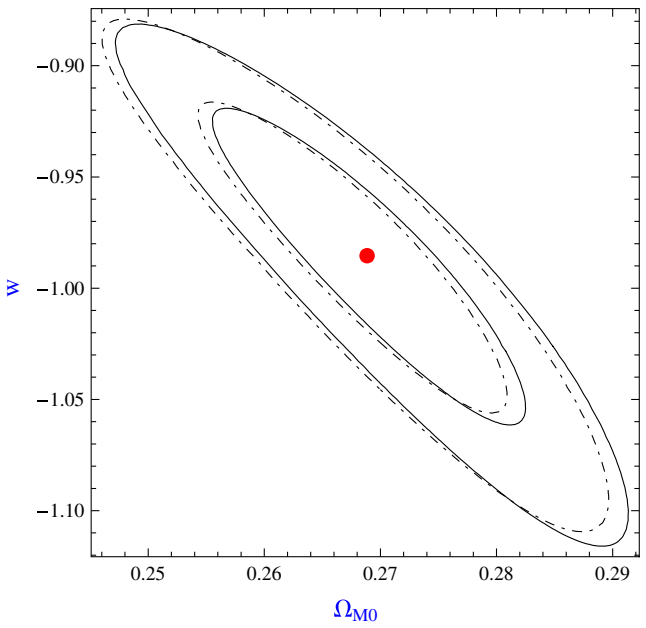

FIG. 3 (color online). The joint confidence regions in the (Ω_{M0}, w) plane for the dark energy model with a constant w for a flat universe with SNe + GRBs + CMB + BAO + CBF + $H(z)$. The contours correspond to 1-σ and 2-σ confidence regions, and the red point is the best-fit value [SNe + GRBs + CMB + BAO + CBF + $H(z)$]. The results for the cases with and without GRBs are indicated by the solid lines and the dot-dashed lines, respectively.

similar to the number of GRBs when including GRBs in the joint fitting. This model has the lowest BIC compared to other models tested from the joint data [357SNe + CMB + BAO + CBF + $H(z)$] with GRBs, so ΔBIC are measured with respect to this model. Figure 3 shows the joint confidence regions in the (Ω_{M0}, w) plane for the wCDM model with a constant EoS for a flat universe. With 357SNe + GRBs + CMB + BAO + CBF + $H(z)$, the 1-σ confidence region for (Ω_{M0}, w) of the flat wCDM model are $(\Omega_M, w) = (0.269^{+0.013}_{-0.014}, -0.99^{+0.07}_{-0.07})$, with $\chi^2_{min} = 494.532$ for 438 degrees of freedom. For comparison, fitting results from the joint data without GRBs are also given in Fig. 3. With 357SNe + CMB + BAO + CBF + $H(z)$, the best-fit values are $(\Omega_{M0}, w) = (0.267^{+0.013}_{-0.014}, -0.98^{+0.07}_{-0.07})$, with $\chi^2_{min} = 448.808$ for 396 degrees of freedom. We present the best-fit value of Ω_{M0}, Ω_Λ with 1σ uncertainties, and χ^2_{min}, χ^2_{min}/dof, as well as AIC, BIC for the flat wCDM model in Table I.

Comparing to the joint constraints with GRBs and without GRBs, we can see that the contribution of GRBs to the joint cosmological constraints is a slight shift when adding the best-fit value of Ω_{M0} to 0.002 and subtracting the best-fit value of w to -0.01 to enclose the ΛCDM model ($w = -1$). From the joint data [357SNe + CMB + BAO + CBF + $H(z)$] with GRBs for the flat wCDM model, we

TABLE I. The best-fit value of Ω_{M0}, Ω_Λ, and w with 1σ uncertainties, and χ^2_{min}, χ^2_{min}/dof, as well as AIC, BIC for the ΛCDM model and for the flat wCDM model with SNe + GRBs + CMB + BAO + CBF + $H(z)$ (with GRBs) and SNe + CMB + BAO + CBF + $H(z)$ (without GRBs).

	ΛCDM model (with GRBs)	ΛCDM model (without GRBs)	wCDM model (with GRBs)	wCDM model (without GRBs)
Ω_{M0}	$0.275^{+0.016}_{-0.015}$	$0.270^{+0.016}_{-0.015}$	$0.269^{+0.013}_{-0.014}$	$0.267^{+0.013}_{-0.014}$
Ω_Λ	$0.723^{+0.017}_{-0.016}$	$0.730^{+0.017}_{-0.017}$	$\Omega_\Lambda \equiv 1 - \Omega_{M0}$	$\Omega_\Lambda \equiv 1 - \Omega_{M0}$
w	$w \equiv -1$	$w \equiv -1$	$-0.99^{+0.07}_{-0.07}$	$-0.98^{+0.07}_{-0.07}$
χ^2_{min}	494.476	449.001	494.532	448.808
χ^2_{min}/dof	1.129	1.134	1.129	1.133
AIC	500.476	454.001	500.532	454.808
BIC	512.736	466.960	512.792	466.767

obtain $\Delta\mathrm{BIC} = 0.056$ with respect to the ΛCDM model. This has the lowest BIC compared to other models tested from the joint data [357SNe + CMB + BAO + CBF + $H(z)$] without GRBs, so ΔBIC are measured with respect to this model. Therefore, for the ΛCDM from the joint data without GRBs, we obtain $\Delta\mathrm{BIC} = 0.193$ with respect to the flat wCDM model.

For the flat CPL model, we find that the best-fit parameters with 357SNe + GRBs + CMB + BAO + CBF + $H(z)$ are $(w_0, w_a, \Omega_{\mathrm{M0}}) = (-0.98, -0.02, 0.269)$, with $\chi^2_{\mathrm{min}} = 494.53$ for 437 degrees of freedom. Figure 4 shows the joint confidence regions in the (w_0, w_a) plane, while fixing $\Omega_{\mathrm{M0}} = 0.269$. For comparison, fitting results from the joint data without GRBs are also given in Fig. 4. With 357SNe + CMB + BAO + CBF + $H(z)$, the best-fit values are $(w_0, w_a, \Omega_{\mathrm{M0}}) = (-0.95, -0.14, 0.269)$, with $\chi^2_{\mathrm{min}} = 448.726/395$. Fitting results with 397SNe + CMB + BAO + CBF + $H(z)$ are also given in Fig. 4 and the best-fit values are $(w_0, w_a, \Omega_{\mathrm{M0}}) = (-0.99, 0.00, 0.269)$, with $\chi^2_{\mathrm{min}} = 504.496/435$. In addition, fitting results from the joint data with 357SNe + GRBs + CMB + BAO, 357SNe + GRBs + BAO, and 357SNe + GRBs + CMB are given in Fig. 5. We note that the contours for 357SNe + GRBs + BAO are sharply cut off at the top, near the line given by $w_0 + w_a = 0$, as shown in the figure. This is due to $w(z \gg 1) < 0$ or $w_0 + w_a < 0$ in the CPL parametrization (i.e., the early universe is matter dominated) implicitly required by the BAO data; this was also noted by Kowalski *et al.* [60]. We present the best-fit value of the derived w_0, w_a with 1σ uncertainties, and the best-fit value of Ω_{M0}, χ^2_{min}, $\chi^2_{\mathrm{min}}/\mathrm{dof}$, as well as AIC, BIC with differently combined data set in Table II.

Comparing to the joint constraints with GRBs and without GRBs, we can see that the contribution of GRBs to the joint cosmological constraints is a slight shift in the (w_0, w_a) plane to enclose the ΛCDM model ($w_0 = -1$, $w_a = -0$). From the joint data [357SNe + CMB + BAO + CBF + $H(z)$] with GRBs for the flat CPL model, we obtain $\Delta\mathrm{BIC} = 6.141$ with respect to the ΛCDM model, indicating a strong preference for the ΛCDM model; while from the joint data without GRBs for the flat CPL model, we obtain $\Delta\mathrm{BIC} = 5.905$ with respect to the flat wCDM model. Meanwhile comparing to Figs. 4 and 5, we find the effects of adding the 26 f_{gas} data and the 11 $H(z)$ data are not very significant, suggesting that the model parameters are strongly constrained by SNe + GRBs + CMB + BAO. Comparing to the joint constraints with SNe + GRBs + CMB and SNe + GRBs + BAO, we find

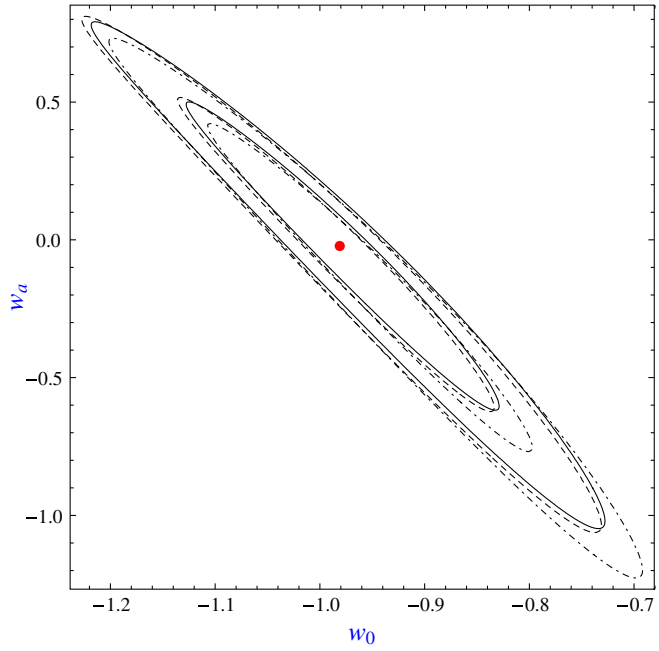

FIG. 4 (color online). The joint confidence regions in the (w_0, w_a) plane for the CPL model in a flat universe with 357SNe + GRBs + others (CMB + BAO + CBF + H), 357SNe + others (without GRBs), and 397SNe + others. The contours correspond to 1-σ and 2-σ confidence regions, and the red point is the best-fit value (357SNe + GRBs + CMB + BAO + CBF + H). The solid lines represent the results of 357SNe + GRBs + others (CMB + BAO + CBF + H). The dash-dotted lines represent the results of 357SNe + others (without GRBs). The dashed lines represent the results of 397SNe + others.

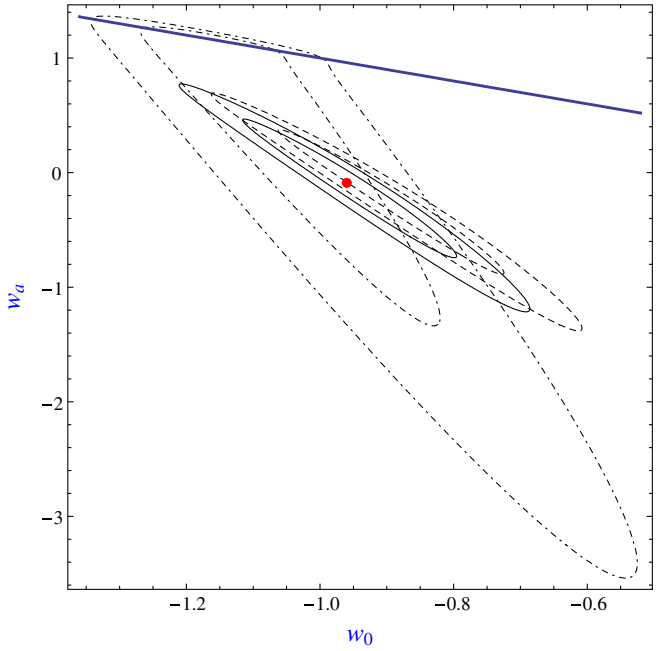

FIG. 5 (color online). The joint confidence regions in the (w_0, w_a) plane for the CPL model in a flat universe with 357SNe + GRBs + CMB + BAO, 357SNe + GRBs + CMB, and 357SNe + GRBs + BAO. The contours correspond to 1-σ and 2-σ confidence regions, and the red point is the best-fit value (357SNe + GRBs + CMB + BAO). The solid lines represent the results of 357SNe + GRBs + CMB + BAO. The dashed lines represent the results of 357SNe + GRBs + CMB. The dash-dotted lines represent the results of 357SNe + GRBs + BAO. The straight line near the top is given by $w_a + w_0 = 0$.

TABLE II. The best-fit value of the corresponding (w_0, w_a) with 1σ uncertainties and the best-fit value of Ω_{M0}, and χ^2_{min}, χ^2_{min}/dof, as well as AIC, BIC for the CPL model in a flat universe, with 357SNe + GRBs + others (CMB + BAO + CBF + H), 357SNe + others (without GRBs), 397SNe + others, and with 357SNe + GRBs + C(CMB) + b(BAO), 357SNe + GRBs + CMB, and 357SNe + GRBs + BAO.

	357SNe + GRB +others	357SNe +others	397SNe +others	357SNe + GRB +C + B	357SNe + GRB + C	357SNe + GRB + B
w_0	$-0.98^{+0.16}_{-0.15}$	$-0.95^{+0.16}_{-0.17}$	$-0.99^{+0.16}_{-0.15}$	$-0.96^{+0.16}_{-0.16}$	$-0.90^{+0.17}_{-0.17}$	$-1.15^{+0.33}_{-0.12}$
w_a	$-0.02^{+0.47}_{-0.60}$	$-0.14^{+0.50}_{-0.65}$	$0.00^{+0.50}_{-0.62}$	$-0.09^{+0.57}_{-0.66}$	$-0.21^{+0.59}_{-0.67}$	$1.06^{+0.18}_{-2.36}$
Ω_{M0}	0.269	0.269	0.269	0.269	0.263	0.307
χ^2_{min}	494.530	448.726	504.496	458.857	455.554	452.839
χ^2_{min}/dof	1.132	1.136	1.160	1.147	1.145	1.138
AIC	502.530	456.726	512.496	464.857	463.554	460.839
BIC	518.877	472.672	528.825	482.853	479.530	476.815

the confidence regions with SNe + GRBs + CMB seem to close to the joint constraints with SNe + GRBs + CMB + BAO. It indicates that the contribution of CMB data to the joint cosmological constraints (SNe + GRBs) is more significant compared to that of BAO data.

From Figs. 2–5 and Tables I and II, we can find that the ΛCDM model is consistent with the joint data in the 1-σ confidence region. Comparing to the joint constraints with GRBs and without GRBs, we can find the effect of GRBs to the joint cosmological constraints, although the contribution of GRBs to the cosmological constraints would not be sufficiently significant compared to that of SNe Ia at present. This is mainly caused by the relatively large statistical scattering in the GRB relations and the relatively small data set of GRBs compared to that of SNe Ia currently.

IV. RECONSTRUCTING THE ACCELERATION HISTORY OF THE UNIVERSE

Following a well-known procedure in the analysis of large scale structure, Shafieloo *et al.* used a Gaussian smoothing function rather than the top hat smoothing function to smooth the noise of the SNe Ia data directly [53,54]. In order to obtain important information on interesting cosmological parameters expediently, when doing the Gaussian smoothing, $\ln d_L(z)$, rather than the luminosity distance $d_L(z)$ or distance modulus $\mu(z)$, is studied by an iterative method [53,54]. Here we follow the iterative procedure and adopt results from Ref. [55],

$$\ln f(z)^s_n = \ln f(z)^s_{n-1} + N(z)\sum_i [\ln f^{\rm obs}(z_i) - \ln f(z_i)^s_{n-1}]N_i(z), \quad (30)$$

where $f(z) \equiv D_L(z)/h$, $f(z)^s_n$ represents the smoothed luminosity distance at any redshift z after the nth iteration, $f(z)^s_0$ denotes a guess background model, and $f^{\rm obs}(z_i)$ is the observed one from the SNe Ia data, as well as the normalization parameter $N(z)^{-1} = \sum_i N_i(z)$, $N_i(z) = \exp[-(\ln^2((1+z)/(1+z_i)))/(2\triangle^2)]$. It has been shown that the results are not sensitive to the chosen value of Δ and the assumed initial guess model. Here we use a wCDM model with $w = -0.9$ and $\Omega_{M0} = 0.28$ as the guessed background model and we choose $\triangle = 0.6$ [55].

The best iterative result is obtained by minimizing

$$\chi^2_n = \sum_i (\mu(z_i)_n - \mu^{\rm obs}(z_i))^2/\sigma^2_{\mu_{{\rm obs},i}}. \quad (31)$$

Once the χ^2_n reaches its minimum value, we stop the iterative process and get the best result (χ^2_{min}), with the 1-σ uncertainties corresponding to $\chi^2 = \chi^2_{min} + 1$. Figure 6 shows the computed χ^2_n for the reconstructed results at each iteration for the SN Ia and GRB data. We find that when at $n = 16$ a minimum value of χ^2_n is obtained.

By using the iterative approach to reconstruct the luminosity distance at any redshift in the redshift range of

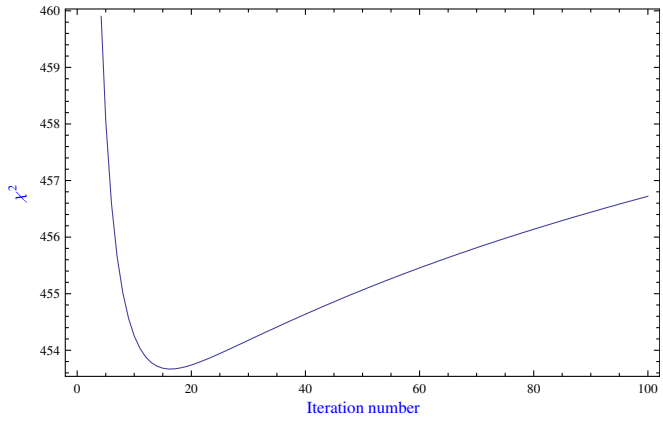

FIG. 6 (color online). Computed χ^2_n for the reconstructed results at each iteration for the SN Ia and GRB data. The minimum value of χ^2_n is obtained at $n = 16$, and the 1-σ uncertainties of reconstructed results can be obtained at $n = 9$, 41, corresponding to $\Delta\chi^2 = 1$, respectively.

SNe Ia, we have calibrated GRB luminosity relations in a model independent manner [52]. Here we reconstruct the Hubble parameter $H(z)$, the deceleration parameter $q(z)$, and the *EoS* of dark energy $w(z)$ from the best iterative result of $f(z)$ with the distance moduli of SNe Ia and GRBs obtained by the interpolating method. The Hubble parameter can be given by differentiating the smoothed luminosity distance [55],

$$H(z) = \left\{\frac{d}{dz}\left[\frac{100f(z)}{(1+z)}\right]\right\}^{-1}, \tag{32}$$

which contains the information on H_0. Then the deceleration parameter $q(z)$ of the expanding universe and the *EoS* of dark energy can be obtained [55],

$$q(z) = (1+z)\frac{H'(z)}{H(z)} - 1, \tag{33}$$

$$w(z) = \frac{-1 + \frac{2}{3}(1+z)\cdot H'/H}{1-(1+z)^3\Omega_{M0}H_0^2/H^2}, \tag{34}$$

where the prime ($'$) denotes the derivative with respect to z.

The reconstructed $H(z)$ with the 1-σ uncertainties are shown in Fig. 7. For comparison, the theoretical values of the ΛCDM model are also shown in Fig. 7. We can find that

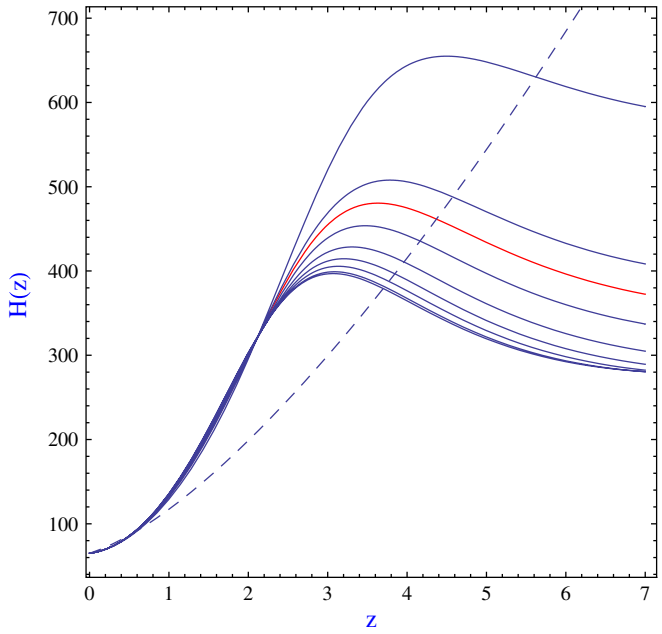

FIG. 7 (color online). The reconstructed $H(z)$ with the 1-σ uncertainties. The red line indicates the best-fit value of the reconstructed $H(z)$, which is obtained at $n = 16$, and the blue lines represent the fit values of the reconstructed $H(z)$ within 1-σ uncertainties at $n = 9, 14, 19, 24, 29, 34, 39, 41$. The dashed line is the theoretical values of the ΛCDM model.

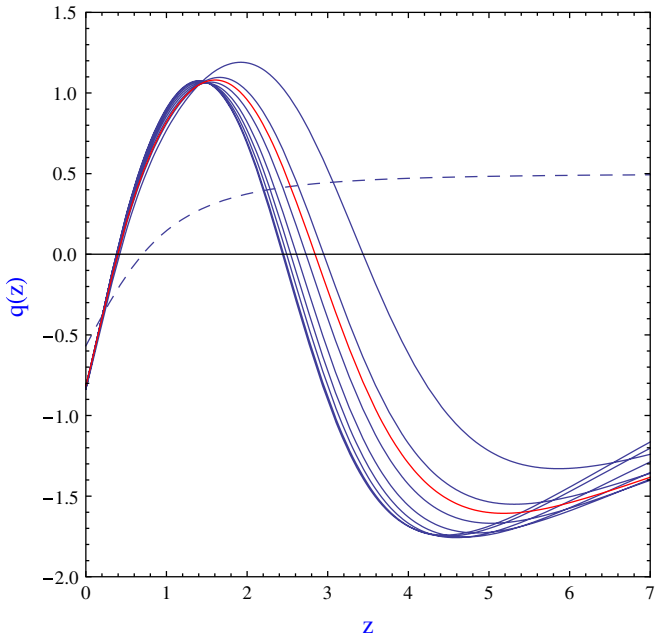

FIG. 8 (color online). The reconstructed $q(z)$ with the 1-σ uncertainties. The red line indicates the best-fit value of the reconstructed $q(z)$, which is obtained at $n = 16$, and the blue lines represent the fit values of the reconstructed $q(z)$ within 1-σ uncertainties at $n = 9, 14, 19, 24, 29, 34, 39, 41$. The dashed line is the theoretical values of the ΛCDM model.

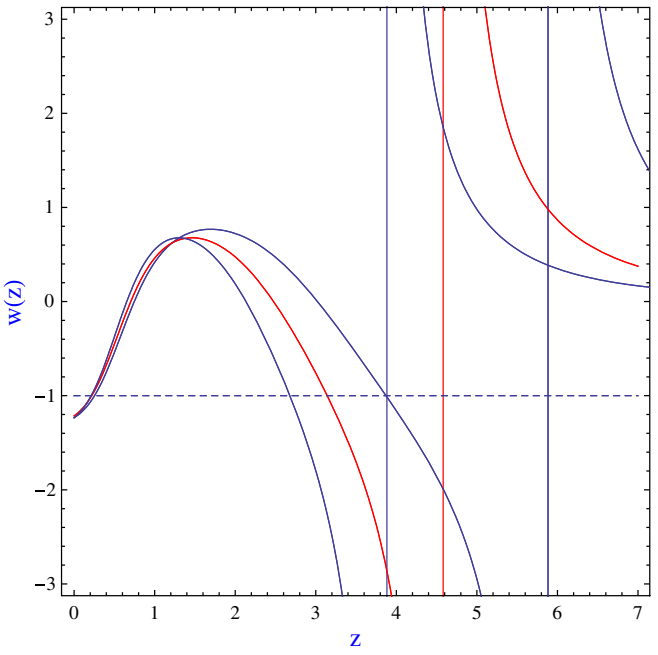

FIG. 9 (color online). The reconstructed *EoS* of dark energy $w(z)$ with the 1-σ uncertainties. The red line indicates the best-fit value of the reconstructed $w(z)$, which is obtained at $n = 16$, and the blue lines represent 1-σ uncertainties at $n = 9, 41$. The dashed line is the theoretical values of the ΛCDM model.

there is a deviation between the reconstructed $H(z)$ and the theoretical values of the ΛCDM model with the 1-σ uncertainty at $1 \lesssim z \lesssim 4$, where the GRB data clearly dominate. The reconstructed $q(z)$ with the 1-σ uncertainties are shown in Fig. 8. We can find that the transition redshift at which the expansion of the universe from deceleration ($q(z) > 0$) to acceleration ($q(z) < 0$) is $z_T = 0.38^{+0.03}_{-0.03}$, at relatively low redshifts, where the SNe Ia data dominate, which is slightly later but more stringent than that reconstructed from the ESSENCE supernova data ($z \sim 0.55 - 0.73$) [55]. However, there is another transition redshift at which the expansion of the universe from acceleration to deceleration, $\tilde{z}_T \simeq 3$, at high redshift where GRB data dominate. However, this transition redshift has large 1-σ uncertainties ($2.4 < \tilde{z}_T < 3.5$) compared to the former one $0.35 < z_T < 0.41$, similar to that reconstructed from the GRB data using the Amati relation [48]. The reconstructed *EoS* of dark energy $w(z)$ with the 1-σ uncertainties are shown in Fig. 9. We can find that there is a singular point at $z \lesssim 5$ from the reconstructed $w(z)$. This phenomenon has been known to happen and just displays the fact that $w(z)$ [Eq. (34)] is nothing more than an effective parameter that (in this case) fails to describe the system correctly. On the other hand, the singular point may be caused by the absence of data in the Hubble diagram at $5 \lesssim z \lesssim 6$, i.e., between the GRB data at $z < 5$ and the only two GRBs at $z > 6$ as shown in Fig. 1.

From Figs. 7–9, we can read that $H_0 = 66\ \mathrm{km\,s^{-1}\,Mpc^{-1}}$, $q_0 = -0.82$, and $w_0 = -1.19$. We can also find some features in the reconstructed $H(z)$, $q(z)$, and $w(z)$, which seem to favor the oscillating models [85–87]. However, it is noted that because the available data of GRBs at high redshift are still quite rare now, and their statistical scatters are relatively large compared to that of SNe Ia, these tentative results might be artifacts, but nevertheless deserve further investigations.

V. SUMMARY AND DISCUSSION

Because of the lack of enough low redshift GRBs to calibrate the luminosity relation, GRBs could not be used reliably and extensively in cosmology until recently. In our previous paper, we have proposed a new method to calibrate GRB luminosity relations in a completely cosmology-independent manner to avoid the well-known circularity problem [45].

In this work, with the recent GRB data at high redshift whose distance moduli are calibrated with the interpolating method [45] from the Union set of 307 SNe Ia [60], as well as the Constitution set of SNe Ia [61], the CMB observation from the WMAP5 result (R, l_a, $\Omega_b h^2$) [62], the BAO observation from the spectroscopic SDSS DR7 galaxy sample ($d_{0.2}$, $d_{0.35}$) [64], the x-ray baryon mass fraction in clusters of galaxies [65], and the observational $H(z)$ data [66,67], we find that the ΛCDM model is consistent with the joint data in 1-σ confidence region; this confirms the conclusion of many previous investigations. We also find that the current GRB data are substantially less accurate than the SNe Ia data, if each data set is used alone, consistent with previous investigations.

The new results and insights we have obtained in this work are briefly summarized as follows:

(1) In order to combine GRB data into the joint observational data analysis to constrain cosmological models, we provide a simple method to avoid any correlation between the SNe Ia data and the GRB data; in this method those SNe Ia data points used for calibrating the GRB data are not used.

(2) Comparing to the joint constraints with GRBs and without GRBs, we find that the contribution of GRBs to the joint cosmological constraints is a slight shift in the confidence regions of cosmological parameters to better enclose the ΛCDM model.

(3) Finally we reconstruct the Hubble parameter $H(z)$, the deceleration parameter $q(z)$, and the *EoS* of dark energy $w(z)$ of the acceleration Universe up to $z > 6$ with the distance moduli of the Constitution set of SNe and GRBs and find some features that seem to favor oscillatory cosmology models; however, further investigations are needed to better understand the situation.

For considering the use of GRBs for cosmology, the gravitational lensing effect may need to be considered [88]. However, Schaefer found that the gravitational biases of GRBs are small [17]. Recently, some possible observational selection bias [89–92] and evolution effects [93–96] in GRB relations have also been discussed. However, Ghirlanda *et al.* confirmed the spectral-energy relations of GRBs observed by *Swift* [97]. Moreover, it is found that instrumental selection effects do not dominate for the Amati relation [98] and for the $E_{\mathrm{peak}} - L$ relation [99], as well as no strong evolution with redshift of the Amati relation can be found [98,100]. Nevertheless, for considering GRBs as standard candles to constrain cosmology, further examinations of possible selection bias and evolution effects should be required in a larger GRB sample.

Different dark energy models may have very different Hubble diagrams at high redshifts [17]. Therefore, the best plan to investigate the property of dark energy is measuring the dark energy over a wide range of redshifts. GRBs can extend the Hubble diagram to much higher redshifts beyond SNe Ia data [17]. It is worth noticing that GRBs are important potential probes for cosmic history up to $z > 6$. However, the contribution of GRBs to the cosmological constraints would not be sufficiently significant at present, due to the large statistical scatters of the relations and the small data set of GRBs. As discussed in [17], GRBs are almost immune to dust extinction, whereas in the case of SNe Ia observations, there is extinction from the interstellar medium when optical photons propagate toward us. On the other hand, SNe Ia are substantially more accurate

standard candles than GRBs, which will lead to tight constraints on cosmological parameters, whereas a single GRB at high redshift will provide more information than a single maximal redshift SNe Ia [17]. Through Monte Carlo simulations, a future prospect of probing dark energy parameters with a larger sample of GRBs has been investigated [8,22,33,59]. It has been found that cosmological constraints would improve substantially with more simulated GRBs expected by future observations. Recently, Xiao and Schaefer have compiled 107 long GRBs with their spectroscopic/photometric redshifts measured [101], observed by BATSE, Konus, HETE, and *Swift*. Along with more and more GRBs observed from *Fermi Gamma-ray Space Telescope* (formerly known as *GLAST*) with much smaller scatters, and its combination with the increasing *Swift* data, GRBs could be used as an additional choice to set tighter constraints on cosmological parameters of dark energy models.

ACKNOWLEDGMENTS

We thank the anonymous referee for comments and suggestions. We also thank Professors Zong-Hong Zhu, Ti-Pei Li, Rong-Gen Cai, Zi-Gao Dai, Ren-Cheng Shang, Zhan Xu, Fang-Jun Lu, En-Wei Liang, and Hongwei Yu for kind help and discussions. N. L. thanks Yun Chen, He Gao, Shuo Cao, Hao Wang, Fang Huang, Jie Ma, Xinjiang Zhu, and Dr. Yi Zhang for discussions. P. X. W. acknowledges partial support by the National Natural Science Foundation of China under Grant No. 10705055, the Program for NCET (No. 09-0144), and the FANEDD under Grant No. 200922. S. N. Z. acknowledges partial funding support by Directional Research Project of the Chinese Academy of Sciences under Project No. KJCX2-YW-T03 and by the National Natural Science Foundation of China under Grants No. 10821061, No. 10733010, No. 10725313, and by 973 Program of China under Grant No. 2009CB824800.

APPENDIX A: THE SN IA DATA USED IN THE INTERPOLATING PROCEDURE FOR CALIBRATING THE GRB DATA

Here we list the 40 SNe Ia data points that have been used to obtain the distance moduli of the 27 GRBs at $z < 1.4$ in the interpolating procedure and have consequently been excluded from the SNe Ia sample used to the joint constraints.

TABLE III. The SNe Ia data points used in the interpolating procedure for calibrating the GRB data at $z < 1.4$. Columns 1 and 2 are SNe Ia used in the interpolating procedure with their redshifts; columns 3 and 4 are the GRB data at $z < 1.4$ with their redshifts.

SN	z_{SN}	GRB	z_{GRB}
1999bp	0.1561	030329	0.17
1996h	0.2130		
1995ao	0.2486	020903	0.25
1995ap	0.2630		
2001hs	0.4300	990712	0.43
2001fs	0.4300		
2001fo	0.4300		
2000fr	0.4300		
1998aw	0.4500	010921	0.45
1998as	0.4500		
1997ez	0.4500		
04D3nc	0.6100	050525	0.61
04D3ny	0.6450	050416	0.65
04D3ml	0.6550		
03D4cn	0.6950	020405	0.70
03D3aw	0.6950	970228	0.70
03D1fl	0.7070	041006	0.71
03D1cm	0.7100	991208	0.71
d097	0.7800	030528	0.78
e108	0.8000	051022	0.80
f076	0.8300	050824	0.83
f096	0.8300	970508	0.84
f235	0.8400	990705	0.84
f244	0.8400	000210	0.85
f308	0.8540		
g050	0.8600	040924	0.86
h364	0.9600	970828	0.96
k411	0.9700	980703	0.97
k425	0.9700		
k485	1.0100	021211	1.01
m027	1.0100		
m062	1.0200	991216	1.02
m138	1.0200		
m193	1.0570	000911	1.06
m226	1.1200	980631	1.10
n278	1.2300	050408	1.24
n285	1.2650	020813	1.25
n326	1.3000	050126	1.29
p454	1.3050	990506	1.31
p455	1.3400		
Number (SN)	40	Number (GRB)	27

[1] N. R. Tanvir *et al.*, Nature (London) **461**, 1254 (2009); R. Salvaterra *et al.*, Nature (London) **461**, 1258 (2009).
[2] L. Amati *et al.*, A&A International **390**, 81 (2002); , Mon. Not. R. Astron. Soc. **372**, 233 (2006).
[3] J. P. Norris, G. F. Marani, and J. T. Bonnell, Astrophys. J. **534**, 248; (2000); T. N. Ukwatta *et al.*, Astrophys. J. **711**, 1073 (2010).
[4] E. E. Fenimore and E. Ramirez-Ruiz (to be published); D. E. Riechart *et al.*, Astrophys. J. **552**, 57 (2001).
[5] B. E. Schaefer, Astrophys. J. **583**, L71 (2003); D.

Yonetoku *et al.*, Astrophys. J. **609**, 935 (2004).
[6] B. E. Schaefer, *Gamma-Ray Bursts: The Brightest Explosions in the Universe* (Harvard, Cambridge, MA, 2002).
[7] G. Ghirlanda, G. Ghisellini, and D. Lazzati, Astrophys. J. **616**, 331 (2004).
[8] E. W. Liang and B. Zhang, Astrophys. J. **633**, 611 (2005).
[9] C. Firmani, V. Avila-Reese, G. Ghisellini, and G. Ghirlanda, Mon. Not. R. Astron. Soc. **370**, 185 (2006); F. Rossi *et al.*, Mon. Not. R. Astron. Soc. **388**, 1284 (2008).
[10] B. Yu, S. Qi, and T. Lu, Astrophys. J. **705**, L15 (2009).
[11] J. Hakkila *et al.*, Astrophys. J. **677**, L81 (2008); Z. B. Zhang, G. Z. Xie, and C. S. Choi, Int. J. Mod. Phys. D **17**, 1391 (2008); R. Sato *et al.*, arXiv:0711.0903; B. Gendre, A. Galli, and M. Boër, AIP Conf. Proc. **1000**, 72 (2008).
[12] R. Willingale *et al.*, arXiv:0710.3727; M. G. Dainotti, V. F. Cardone, and S. Capozziello, Mon. Not. R. Astron. Soc. **391**, L79 (2008); S. Qi and T. Lu, arXiv:0911.5248.
[13] R. Tsutsui *et al.*, J. Cosmol. Astropart. Phys. 08 (2009) 015.
[14] B. Zhang, Chin. J. Astron. Astrophys. **7**, 1 (2007).
[15] B. E. Schaefer and A. C. Collazzi, Astrophys. J. **656**, L53 (2007).
[16] G. Ghirlanda, G. Ghisellini, and C. Firmini, New J. Phys. **8**, 123 (2006).
[17] B. E. Schaefer, Astrophys. J. **660**, 16 (2007).
[18] B. E. Schaefer, Astrophys. J. **583**, L67 (2003).
[19] J. S. Bloom, D. A. Frail, and S. R. Kulkarni, Astrophys. J. **594**, 674 (2003).
[20] Z. G. Dai, E. W. Liang, and D. Xu, Astrophys. J. **612**, L101 (2004).
[21] G. Ghirlanda, G. Ghisellini, D. Lazzati, and C. Firmini, Astrophys. J. **613**, L13 (2004).
[22] D. Xu, Z. G. Dai, and E. W. Liang, Astrophys. J. **633**, 603 (2005).
[23] C. Firmani, G. Ghisellini, G. Ghirlanda, and V. Avila-Reese, Mon. Not. R. Astron. Soc. **360**, L1 (2005).
[24] C. Firmani, V. Avila-Reese, G. Ghisellini, and G. Ghirlanda, Mon. Not. R. Astron. Soc. **372**, L28 (2006); Rev. Mex. Astron. Astrofis. **43**, 203 (2007).
[25] A. S. Friedman and J. S. Bloom, Astrophys. J. **627**, 1 (2005); T. Di Girolamo *et al.*, J. Cosmol. Astropart. Phys. 04 (2005) 008; D. Hooper and S. Dodelson, Astropart. Phys. **27**, 113 (2007).
[26] F. Y. Wang and Z. G. Dai, Mon. Not. R. Astron. Soc. **368**, 371 (2006); H. Li *et al.*, Phys. Lett. B **658**, 95 (2008); M. Su, Z. H. Fan, and B. Liu, arXiv:astro-ph/0611155; H. J. Mosquera Cuesta *et al.*, arXiv:astro-ph/0609262; arXiv:astro-ph/0610796.
[27] H. J. Mosquera Cuesta *et al.*, J. Cosmol. Astropart. Phys. 07 (2008) 004; A&A International **487**, 47 (2008).
[28] S. Basilakos and L. Perivolaropoulos, Mon. Not. R. Astron. Soc. **391**, 411 (2008).
[29] E. L. Wright, Astrophys. J. **664**, 633 (2007); R. A. Daly *et al.*, Astrophys. J. **677**, 1 (2008); V. Vitagliano *et al.*, J. Cosmol. Astropart. Phys. 03 (2010) 005.
[30] F. Y. Wang, Z. G. Dai, and Z. H. Zhu, Astrophys. J. **667**, 1 (2007); F. Y. Wang and Z. G. Dai, AIP Conf. Proc. **1065**, 373 (2008); F. Y. Wang, Z. G. Dai, and S. Qi, Res. Astron. Astrophys. **9**, 547 (2009).
[31] Y. Gong and X. Chen, Phys. Rev. D **76**, 123007 (2007).
[32] S. Qi, F. Y. Wang, and T. Lu, A&A International **483**, 49 (2008); **487**, 853 (2008).
[33] K. Takahashi *et al.*, arXiv:astro-ph/0305260.
[34] O. Bertolami and P. T. Silva, Mon. Not. R. Astron. Soc. **365**, 1149 (2006).
[35] C. Firmani, V. Avila-Reese, G. Ghisellini, and G. Ghirlanda, Mon. Not. R. Astron. Soc. **372**, L28 (2006).
[36] D. Q. Lamb *et al.*, arXiv:astro-ph/0507362 (to be published).
[37] G. Ghirlanda *et al.*, A&A International **452**, 839 (2006).
[38] E. W. Liang and B. Zhang, Mon. Not. R. Astron. Soc. **369**, L37 (2006).
[39] H. Li *et al.*, Astrophys. J. **680**, 92 (2008).
[40] L. Amati *et al.*, Mon. Not. R. Astron. Soc. **391**, 577 (2008).
[41] Y. Wang, Phys. Rev. D **78**, 123532 (2008).
[42] S. Qi, T. Lu, and F. Y. Wang, Mon. Not. R. Astron. Soc. **398**, L78 (2009).
[43] L. Samushia and B. Ratra, arXiv:0905.3836.
[44] Y. Wang, Phys. Rev. D **80**, 123525 (2009).
[45] N. Liang, W. K. Xiao, Y. Liu, and S. N. Zhang, Astrophys. J. **685**, 354 (2008).
[46] S. Capozziello and L. Izzo, A&A International **490**, 31 (2008).
[47] L. Izzo *et al.*, Astron. Astrophys. **508**, 63 (2009); arXiv:0906.4888; L. Izzo and S. Capozziello, Nucl. Phys. B, Proc. Suppl. **194**, 206 (2009).
[48] H. Wei and S. N. Zhang, Eur. Phys. J. C **63**, 139 (2009).
[49] H. Wei, Eur. Phys. J. C **60**, 449 (2009).
[50] T. S. Wang and N. Liang, arXiv:0910.5835.
[51] M. Visser, Classical Quantum Gravity **21**, 2603 (2004).
[52] N. Liang and S. N. Zhang, AIP Conf. Proc. **1065**, 367 (2008).
[53] A. Shafieloo, U. Alam, V. Sahni, and A. Starobinsky, Mon. Not. R. Astron. Soc. **366**, 1081 (2006).
[54] A. Shafieloo, Mon. Not. R. Astron. Soc. **380**, 1573 (2007).
[55] P. Wu and H. Yu, J. Cosmol. Astropart. Phys. 02 (2008) 019.
[56] V. F. Cardone, S. Capozziello, and M. G. Dainotti, Mon. Not. R. Astron. Soc. **400**, 775 (2009).
[57] V. F. Cardone, A. Diaferio, and S. Camera, arXiv:0907.4689.
[58] Y. Kodama *et al.*, Mon. Not. R. Astron. Soc. **391**, L1 (2008).
[59] R. Tsutsui *et al.*, Mon. Not. R. Astron. Soc. **394**, L31 (2009).
[60] M. Kowalski *et al.*, Astrophys. J. **686**, 749 (2008).
[61] M. Hicken *et al.*, Astrophys. J. **700**, 1097 (2009).
[62] E. Komatsu *et al.*, Astrophys. J. Suppl. Ser. **180**, 330 (2009).
[63] D. J. Eisenstein *et al.*, Astrophys. J. **633**, 560 (2005).
[64] W. J. Percival *et al.*, Mon. Not. R. Astron. Soc. **401**, 2148 (2010).
[65] S. W. Allen *et al.*, Mon. Not. R. Astron. Soc. **353**, 457 (2004); S. W. Allen, R. W. Schmidt, and A. C. Fabian, Mon. Not. R. Astron. Soc. **334**, L11 (2002).
[66] J. Simon, L. Verde, and R. Jimenez, Phys. Rev. D **71**, 123001 (2005).
[67] E. Gaztañaga, A. Cabré, and A. L. Hui, Mon. Not. R. Astron. Soc. **399**, 1663 (2009).

[68] P. Astier *et al.*, A&A International **447**, 31 (2006).
[69] W. M. Wood-Vasey *et al.*, Astrophys. J. **666**, 694 (2007).
[70] A. G. Riess *et al.*, Astrophys. J. **659**, 98 (2007).
[71] T. M. Davis *et al.*, Astrophys. J. **666**, 716 (2007).
[72] R. Sari, T. Piran, and J. P. Halpern, Astrophys. J. **519**, L17 (1999).
[73] S. Nesseris and L. Perivolaropoulos, Phys. Rev. D **72**, 123519 (2005).
[74] W. Hu and N. Sugiyama, Astrophys. J. **471**, 542 (1996).
[75] J. C. Bueno Sanchez, S. Nesseris, and L. Perivolaropoulos, J. Cosmol. Astropart. Phys. 11 (2009) 029;
[76] D. Eisenstein and W. Hu, Astrophys. J. **496**, 605 (1998).
[77] S. Nesseris and L. Perivolaropoulos, J. Cosmol. Astropart. Phys. 01 (2007) 018.
[78] P. Wu and H. Yu, J. Cosmol. Astropart. Phys. 10 (2007) 014.
[79] R. G. Abraham *et al.* (GDDS Collaboration), Astron. J. **127**, 2455 (2004).
[80] L. A. Nolan *et al.*, Mon. Not. R. Astron. Soc. **341**, 464 (2003); T. Treu *et al.*, Astrophys. J. **564**, L13 (2002)Mon. Not. R. Astron. Soc. **326**, 221 (2001); H. Spinrad *et al.*, Astrophys. J. **484**, 581 (1997); J. Dunlop *et al.*, Nature (London) **381**, 581 (1996).
[81] H. Akaike, IEEE Trans. Autom. Control **19**, 716 (1974).
[82] G. Schwarz, Ann. Stat. **6**, 461 (1978).
[83] A. R. Liddle, Mon. Not. R. Astron. Soc. **351**, L49 (2004).
[84] M. Chevallier and D. Polarski, Int. J. Mod. Phys. D **10**, 213 (2001); E. V. Linder, Phys. Rev. Lett. **90**, 091301 (2003).
[85] G. Barenboim, O. Mena, and C. Quigg, Phys. Rev. D **71**, 063533 (2005); S. Nojiri and S. D. Odintsov, Phys. Lett. B **637**, 139 (2006); E. V. Linder, Astropart. Phys. **25**, 167 (2006).
[86] B. Feng, M. Li, Y. S. Piao, and X. Zhang, Phys. Lett. B **634**, 101 (2006); J. Q. Xia, B. Feng, and X. Zhang, Mod. Phys. Lett. A **20**, 2409 (2005); J. Liu, H. Li, J. Xia, and X. Zhang, J. Cosmol. Astropart. Phys. 07 (2009) 017.
[87] H. Wei and S. N. Zhang, Phys. Lett. B **644**, 7 (2007); H. Wei and S. N. Zhang, Phys. Lett. B **654**, 139 (2007).
[88] M. Oguri and K. Takahashi, Phys. Rev. D **73**, 123002 (2006).
[89] N. R. Butler *et al.*, Astrophys. J. **671**, 656 (2007); **694**, 76 (2009).
[90] F. Fiore *et al.*, A&A International **470**, 515 (2007).
[91] S. Campana *et al.*, A&A International **472**, 395 (2007).
[92] A. Shahmoradi and R. J. Nemiro, arXiv:0904.1464; L. X. Li, Acta Astronomica **58**, 103 (2008).
[93] L. X. Li, Mon. Not. R. Astron. Soc. **379**, L55 (2007); arXiv:0705.4401.
[94] R. Tsutsui *et al.*, Mon. Not. R. Astron. Soc. **386**, L33 (2008).
[95] R. Salvaterra *et al.*, Mon. Not. R. Astron. Soc. **396**, 299 (2009).
[96] V. Petrosian, A. Bouvier, and F. Ryde, arXiv:0909.5051.
[97] G. Ghirlanda *et al.*, A&A International **466**, 127 (2007).
[98] G. Ghirlanda *et al.*, Mon. Not. R. Astron. Soc. **387**, 319 (2008).
[99] G. Ghirlanda *et al.*, A&A International **511**, A43 (2010).
[100] J. Wang, J. S. Deng, and Y. L. Qiu, Chin. J. Astron. Astrophys. **8**, 255 (2008).
[101] L. Xiao and B. E. Schaefer, Astrophys. J. **707**, 387 (2009).